Biosensors and Bioelectronics 168 (2020) 112525

Contents lists available at ScienceDirect

Biosensors and Bioelectronics

journal homepage: http://www.elsevier.com/locate/bios

Normal-incidence type solution immersed silicon (SIS) biosensor for ultra-sensitive, label-free detection of cardiac troponin I

Dong Hyung Kim [a,1], Won Chegal [b,1], Yong Jai Cho [b], Sang Won O [a,c], Long Van Le [a,d], Mangesh S. Diware [e], Se-Hwan Paek [c], Young Dong Kim [d], Hyun Mo Cho [a,*]

[a] Division of Interdisciplinary Materials Measurement Institute, Korea Research Institute of Standards and Science, 267 Gajeongno, Yuseong-Gu, Daejeon, 34113, South Korea
[b] Division of Advanced Instrumentation Institute, Korea Research Institute of Standards and Science, 267 Gajeongno, Yuseong-Gu, Daejeon, 34113, South Korea
[c] Department of Bio-Microsystem Technology, Korea University, Seoul, 02841, South Korea
[d] Department of Physics, Kyung Hee University, Seoul, 02447, South Korea
[e] CeNSCMR and Institute of Applied Physics, Department of Physics and Astronomy, Seoul National University, Seoul, 08826, South Korea

ARTICLE INFO

Keywords:
Solution immersed silicon
Ellipsometry
Normal-incidence prism
Cardiac troponin I
Myocardial infarction

ABSTRACT

Early diagnosis of acute myocardial infarction (AMI) significantly reduce the mortality rate and can be achieved via high-sensitive detection of AMI specific cardiac troponin I (cTnI) biomarker. Here, we present normal-incident type solution-immersed silicon (NI–SIS) ellipsometric biosensor, designed for ultra-high sensitive, high-throughput, label-free detection of the target protein. The NI–SIS sensors are equipped with a specially designed prism that maintains the angle of incidence close to the Brewster angle during operation, which significantly reduces SIS noise signals induced by the refractive index fluctuations of the surrounding medium, improves the signal-to-noise ratio, in-results lowers the detection limit. We applied NI–SIS biosensor for ultra-sensitive detection of cTnI biomarkers in human serum. The optimized sensor chip fabrication and detection operation procedures are proposed. The wide linear concentration ranges of fg/mL to ng/mL is achieved with the detection limit of 22.0 fg/mL of cTnI. The analytical correlation was assessed by linear regression analysis with the results of the Pathfast reference system. These impressive biosensing capabilities of NI–SIS technology have huge potentials for accurate detection of target species in different application areas, such as diagnosis, drug discovery, and food contaminations.

1. Introduction

The human body releases the specific proteins in the bodily fluids on any damage to the internal organs (Bidin et al., 2019), and these biomarkers are the key to detect those damages. Early stages of dangerous chronic and heart diseases are silent in most cases, makes it very difficult to identify these inflections. High-sensitive detection of specific biomarkers is crucial for accurate diagnosis and proper treatment (Lee et al., 2019).

A heart attack happens when a blockage in the coronary arteries limits the oxygen supply, which damages the heart muscles, medically known as an acute myocardial infarction (AMI) (Diware et al., 2017b; Hofmann et al., 2017). The AMI is a life-threatening condition; millions of people losses their lives, and the number is continuously increasing due to the modern lifestyle. AMI biomarker proteins are myoglobin, creatine kinase MB isoform (CK-MB), and cardiac troponin I (cTnI). Early detection of these cardiac markers is crucial to increase the survival chances of AMI patients (Lewandrowski et al., 2002). Myoglobin is an early biomarker, appears 1–3 h in the bloodstream after the event, and has been used to detect the reinfarction (Hasic et al., 2006; Kim et al., 2012). However, Myoblobin has a very low specificity for AMI since it is an oxygen-binding carrier found in all muscle tissues (Kim et al., 2014). The cardiac troponin I (cTnI) is a gold standard for AMI diagnosis, appears in the bloodstream within 4–6 h with peak levels occurring at 18–24 h after the AMI onset, and clinical cut-off value is recommended of <0.1 ng/mL (Madsen et al., 2006). The highly sensitive analysis of cTnI can provide prognostic information supporting risk stratification as well as highly accurate diagnostics at the early stage

* Corresponding author.
E-mail address: hmcho@kriss.re.kr (H.M. Cho).
[1] These authors contributed equally to this work.

https://doi.org/10.1016/j.bios.2020.112525
Received 18 May 2020; Received in revised form 14 August 2020; Accepted 17 August 2020
Available online 21 August 2020

(Lim et al., 2015; Morrow et al., 2000). The clinical sensitivity and specificity of high-sensitive cTnI (hs-cTnI) have been reported to 90.7% and 90.2%, respectively, for AMI (Keller et al., 2009).

Biosensing techniques are continually evolving to enhance analytical performance with signal amplification for target biomarkers directly from blood. Various tracers are used to generate or amplify the sensor signal, such as nanoparticles, enzymes, and fluorescent materials (Deng et al., 2014; Lai et al., 2016; Tan et al., 2017). Fig. S1 presents the detection limit comparison of the ultra-sensitivity troponin assays between present work and various studies in the literature. For example, Yola and Atar fabricated hs-cTnI biosensing technique based on boron nitride quantum dots incorporated with a molecularly imprinted polymer (Yola and Atar, 2019). The imprinted biosensor shows a detection limit of 0.5 pg/mL for cTnI in plasma samples. Tan et al. showed a sensitive detection of cTnI biomarkers with low concentration of 1.8 pg/mL using photoresponsive nanocomposites made from N-acetyl-L-cysteine capped CdAgTe quantum dots and dodecahedral gold nanoparticles (Tan et al., 2017). The polymeric complex of enzymes widely used as the signal generator on enzyme immunoassay (e.g., enzyme-linked immunosorbent assay, ELISA) because it has the superior catalytic activity and substrate specificity (Cho et al., 2018), significantly improve the analytical sensitivity (Lim et al., 2015). However, these enzyme reactions need a lengthy incubation process to induce catalysis with the substrate and can interfere with the sample matrix containing the analyte (Cho et al., 2018). Another approach is the use of fluorophores to produce a sensitive detectable signal in luminescence form. It could detect analyte concentrations in the nM scale with a proper choice of dyes and tagging complexes, such as fluoresce resonance energy transfer (FRET) (Shi et al., 2015). The quenching effect in the FRET might limit the capability of the biosensors because of a high density and complicated format of the traditional fluorophores (Seo et al., 2016). Ortiz-Riaño et al. have overcome these issues by applying a novel immunosensing approach based on graphene oxide (GO)-coated microwells with highly FRET capabilities between photoexcited fluorophores (donors) and GO (acceptor) (Ortiz-Riaño et al., 2020). The fluorophore bound to antibodies (Fl-Abs) has a relatively long distance from the GO-coated surface by a binding reaction between antibody and analyte, generating a sensitive signal by the weakly quench of the fluorophore than that of the unbound Fl-Abs.

Label-free sensing technique does not need any other foreign compound for target detection, has advantageous real-time monitoring of the molecular interaction, and obtain analytical information (Esfandyarpour et al., 2013; Kim et al., 2017). The popular label-free optical sensor is based on surface plasmon resonance (SPR), which can provide highly sensitive signals from the refractive index (RI) changes induced by binding reactions of biomolecules over a thin gold layer (Yanase et al., 2010). The RI of the SPR sensing assembly (biomolecule/gold) is extremely sensitive to temperature (Xiao et al., 2010). The subtle fluctuations in temperature can induce a detectable signal in the SPR system, which could mask the actual binding signal. Hence, thermal noise is a severe limitation for SPR based sensor systems. Separate reference channel is used to account the thermal noise (Kim et al., 2014; Liu et al., 2015), but some avoidable amount is always there.

We are presenting an ultra-sensitive biosensing technique; solution-immersed silicon (SIS) sensor with specially design prism called a normal incidence (NI) prism, named as a NI–SIS sensor. The NI-prism maintains the constant angle of incidence of the probing laser beam on the sensor chip. The NI-prism served two purposes: eliminate the RI noise from surrounding conditions (temperature and pressure) and minimize the strong stray light reflected from the prism surface, which allows to archive high signal-to-noise ratio. The NI-prim is equipped with multiple channels, could be used for reference, reproducibility, or multiple target detection. These analytical properties of the NI–SIS sensor were applied to real-time ultrasensitive detections of the cTnI in human serum. Critical parameters in the optimization of sensor chip fabrication and bio-interaction measurement procedures are discussed.

2. Materials and methods

2.1. Materials

The *p*-type <100> silicon wafers obtained from MCL Electronics Materials, Ltd., China. Human cTnI (from heart tissue 8T53), cardiac troponin I–T–C complex (cTnI-T-C; from heart tissue 8T62), troponin C (cTnC; 8T57), skeletal muscle troponin I (skTnI; 8T25), and a monoclonal antibody to cTnI (clone 19C7) were provided from Hytest Ltd., Finland. 3-Aminopropyl triethoxysilane (APTES), carboxymethyl dextran (CM-dextran) sodium salt, N-hydroxysuccinimide (NHS), ethanolamine, ethanol absolute, casein (from bovine milk), bovine serum albumin (BSA), and human serum (from human male AB plasma) were purchased from Sigma-Aldrich Korea Ltd. Octet red streptavidin (SA) sensor tip and NHS-LC-LC-biotin were obtained from Fortebio (San Francisco, CA, USA) and Pierce (Rockford, IL, USA), respectively. 1-(3-Dimethylaminopropyl)-3-ethalcarbodimide hydrochloride (EDC) was from Tokyo Chemical Industry Co., Ltd. Phosphate buffer solution (PBS; 0.004M phosphate buffer and 0.155M NaCl, pH7.4) was from Gibco, Thermo Fisher Scientific Korea Ltd. All the reagents used in this study were of analytical grade.

2.2. NI–SIS sensor system

The NI–SIS sensor is equipped with specially designed NI prism, shown in Fig. 1, effectively improves the signal-to-noise ratio, helped to archive several hundred-fold increase in detection limit for AMI biomarkers than our previous work (Diware et al., 2017b). Biomolecular interactions are detected using in-house single wavelength ellipsometer. Details of NI–SIS sensor designs are given in the next section.

2.3. Fabrication of sensor chip

The sensor chips are fabricated from *p*-type Si wafers (11.5 mm × 11.5 mm) with a SiO_2 overlayer of different thicknesses (2.0 nm and 52.4 nm), were treated sequentially by the silane and dextran to grow the self-assembled monolayer (SAM) with a functional group. The Si chips were first washed using ethanol to remove surface contaminants and then immersed in a solution of 2 vol % APTES in ethanol for 12 h at room temperature (Aissaoui et al., 2012). Excess APTES was washed using deionized (DI) water, and then CM-dextran (0.1 g/mL) was grown over the silane-SAM to provide highly dense binding sites. Thicknesses of the SiO_2, APTES, and CM-dextran layers on Si wafer were measured by using spectroscopic M2000D ellipsometer from J.A. Woollam co. The spectroscopic ellipsometry (SE) measurements were performed within a wavelength range of 207–826 nm at three angles of incidence of 65°, 70°, and 75°, and data was analyzed using WVASE32 software.

2.4. The specificity of capture antibody

The target specificity of the capture antibody was examined using a label-free sensor system, Octet Red (ForteBio), according to the manufacturer's protocol. The antibody (1 μg/mL) was first biotinylated by targeting the amine groups and then immobilized by biotin-avidin linkages on the Octet SA sensor tip (Kim et al., 2012). The surface combined with the antibody was associated with the cTnI (100 ng/mL) diluted in PBS containing 0.5% casein (Casein-PBS) for 900 s. The cross-reactions were measured repeatedly with negative samples containing skTnI and cTnC, respectively, in the same manner. In a direct assay, the binding signals were provided as a thickness difference of the tip and then were analyzed using the analysis program (Data Analysis 6.3) provided by the manufacturer.

2.5. Functionalization of the sensor chip and analyte detection procedure

The sensor chip modified with carboxylic functional groups of

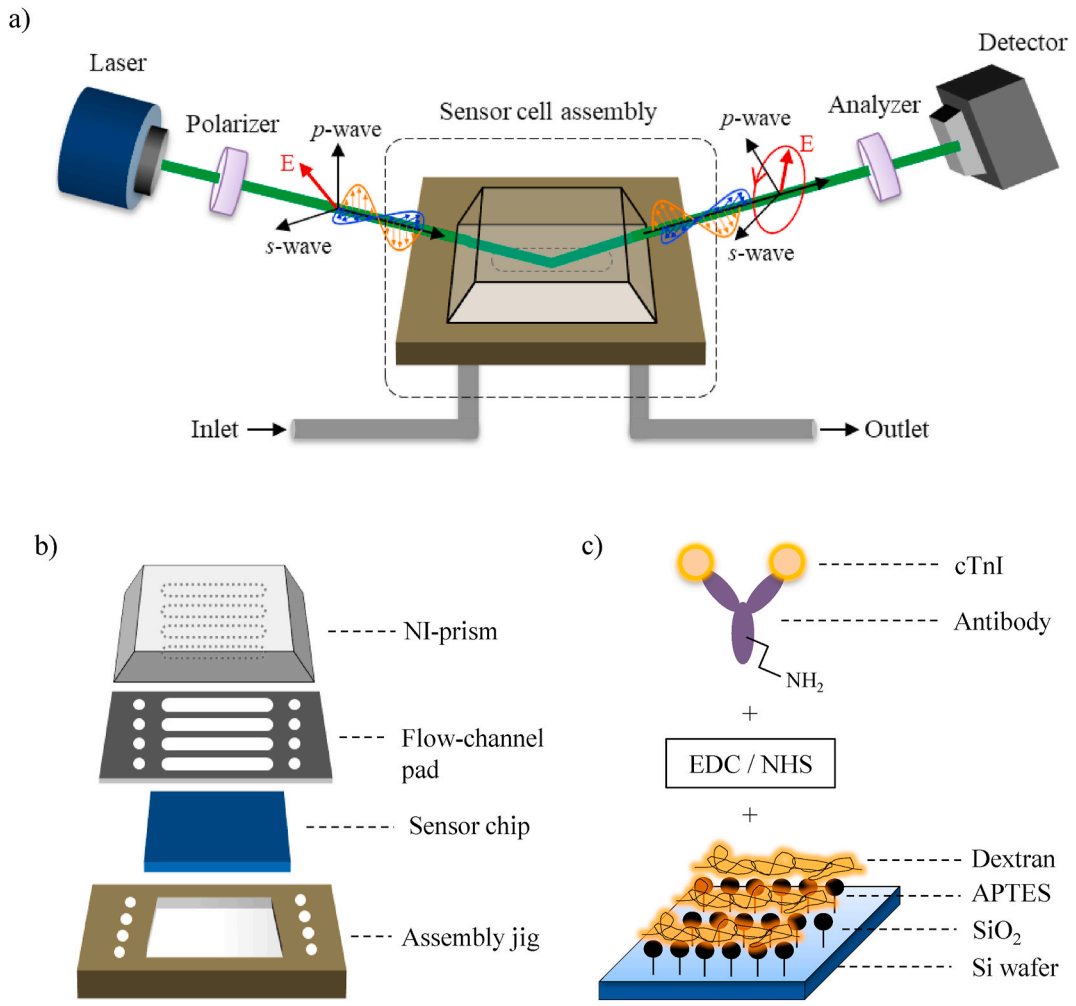

Fig. 1. Schematics of NI–SIS sensor system. (a) The design of the NI–SIS sensor system arranged as a single wavelength (520 nm) laser, fixed polarizer, sensor assembly, rotating analyzer, and detector. (b) The NI–SIS sensor assembly consists of NI-prism, flow-channel pad, sensor chip, and assembly jig. (c) Biomolecular assembly over the sensor surface. The capture antibody was bound covalently with carboxyl groups of dextran-SAM, which used to detect cTnI antigen.

dextran-SAM was docked with NI-prism to construct a sensor cell assembly, as shown in Fig. 1b. The cTnI antibody (25 μg/mL) with NHS and EDC was injected over the sensor chip at a rate of 30 μL/min for 600 s to provide the specific binding sites for cTnI antigen. The unbound molecules were removed by the PBS washing, and the residual active sites were eliminated by flowing the blocking solution of 1M ethanolamine hydrochloride (pH8.5), mixture of 0.5% BSA and PBS (BSA-PBS), and Casein-PBS, respectively. Finally, the sensor surface was cleaned and stabilized by flushing with PBS or 10% human serum.

To detect the cTnI antigens in a direct assay: samples containing cTnI-T-C complex were first prepared with different concentrations in a dilution buffer of PBS and BSA-PBS, respectively. Each sample was sequentially injected over the sensor surface coupled with cTnI antibody at a flow rate of 30 μL/min, and the binding events were measured as the change in ellipsometric angles in real-time. The dose-response curves were measured for the concentrations from 10 fg/mL to 100 ng/mL by spiking the cTnI-T-C stock in normal serum. The serum samples were pretreated with BSA-PBS in a dilution ratio of 1:10 and then were injected over the sensor surface. The unbound antigens were washed using PBS for 200 s. The reactive values for cTnI concentrations were subtracted by the non-specific signals of normal serum and were obtained by averaging the measured signal for 100 s at the washing step.

2.6. Correlation test

The analytical performance of the NI–SIS sensor is verified with the results of Pathfast as a reference system (Di Serio et al., 2009; Seo et al., 2016). The Pathfast analyzer determines the cTnI concentrations quantitatively by a chemiluminescence enzyme immunoassay (CLEIA). The biosensing capability has amplified by providing an efficient bound/free separation process with magnetic particles. The samples were first prepared by adding 50 fg/mL-20 ng/mL cTnI-T-C in normal serum, pretreated with a 10-fold volume of BSA-PBS. The reactive signal from the NI–SIS sensor was converted to the cTnI concentration using a linearized standard curve. The same sample was simultaneously detected using the reference analyzer following the manufacturer's protocol. The two quantitative results were plotted (Fig. 6) on each axis to establish the correlation via linear regression analysis.

3. Results and discussions

3.1. NI–SIS based biosensing technique

NI–SIS sensor uses ellipsometry as a sensing technique. Ellipsometry is the most surface sensitive optical technique known today and has been widely applied to measure the optical properties of materials (Li et al., 2018; Ostroff et al., 1998). It measures the change of polarization state of incident light upon reflection from sensor surface in terms of two

parameters; amplitude ratio (Ψ) and phase difference (Δ) between *s*- and *p*-polarized light, as shown in Fig. 1a. (Bader et al., 1998; Cho et al., 2016; Minamikawa et al., 2017). The *p*- (*s*-) polarization means the electric field vector is aligned in parallel (perpendicular) to the plane of incidence. At the Brewster angle, that is the non-reflecting condition (NRC) for *p*-polarized wave, Ψ is ultra-sensitive to the thickness of the growing bio-layer while Δ almost remains unchanged (Diware et al., 2015). Therefore, Ψ can be used as a sensing signal for detecting the affinity binding between biomolecules (Diware et al., 2017b; Li et al., 2018).

As shown in Fig. 1a, Optical components in the NI–SIS sensor system are arranged as: probing laser, fixed polarizer, sensor assembly, rotating analyzer, and detector. The incident beam (λ = 520 nm) with 40 mW laser diode, purchased from Delos laser Co., Korea, was employed to enhance the signal-to-noise ratio of sensing signals. The excessively high laser power might damage the biomolecules, and can increase the thermal noise by heating the surrounding liquid in the sensing chamber. The light beam has linearly polarized light within 2° with respect to the plane of incidence from the polarizer (Dung et al., 2019). The polarization angle of the probing beam was adjusted closely to the Ψ values of SIS to minimize any errors produced by a non-linearity and gain change of the detector. The NI–SIS assembly is the most important part of the NI–SIS sensor system, where specific binding reactions of target biomolecules happens and probing laser interacts with sensor chip, composes of specially designed NI prism, flow-channel pad, sensor chip, and assembly jig, shown in Fig. 1b. The NI prism facilitates a normal-incidence of the probing beam to every surface of the prism, which maintains the angle of incidence onto the sensor chip close to the Brewster angle. Therefore, NI prism helps to achieve a high signal-to-noise ratio by eliminating a stray noise coming from reflected light from the prism surface (Diware et al., 2017a). The flow channels were constructed by sandwiching patterned polydimethylsiloxane (PDMS) between NI-prism and sensor chip, as shown in Fig. 1b. Desired solutions with antibody and antigen can be injected over the carboxyl-terminated active sensor chip surface using a programmable pump, as shown in Fig. 1c. The Ψ signal provides the information about the thickness change by a binding event between antibody and cTnI antigen at the NRC for *p*-polarized wave (Diware et al., 2015).

3.2. Construction of normal incidence prism

The NI-prism was fabricated from four fused silica parts, as shown in Fig. S2a; indicated in a different color. The four parts are attached to each other by an optical adhesive, providing sensing chambers for holding target-antigen solutions. Sensing chambers (1.5 mm × 6.0 mm x 0.5 mm) are trapezoid shape with two 72° inclined sidewalls (Fig. S2b), gives the highest signal-to-noise ratio in our SIS design. Flow channels were constructed using patterned PDMS pad between NI-prims and sensor chip. The laser spot was focused within a diameter of 1 mm to fit the window areas, and careful alignment is required to remove noise from scattering with other parts of the NI-prism.

Fig. 2a shows the vertical cross-section of NI-prism sensor assembly, designed such a way that the probing beam remains perpendicular to the prism surface, which helps to maintains the angle of incidence close to NRC, in our case at 72.4°. The inclined beam has interacted with the sensor chip surface in an elliptic shape between a major axis of <1.6 mm and a minor axis of <1.0 mm. NI-prism serves two primary purposes; it removes the interference noise by internally reflected beams from the prism surface (dashed red line in Fig. 2b) and reduces analytical errors induced from the incidence angle variations by the refractive index fluctuations of surrounding environments (dashed blue line in Fig. 2b). These are the issues with SIS sensor design with the ordinary prism applied in our previous works (Diware et al., 2017b; Dung et al., 2019), as shown in Fig. 2b. Also, four flow channels are the part of NI-prism, which acts as a reservoir of the binding species during operation, improves the binding amount. Extra space in the flow-channel helps to reduce a flow-pressure, which in-effect reduces the refractive index fluctuations from pressure variations. In results, NI-prism improves the

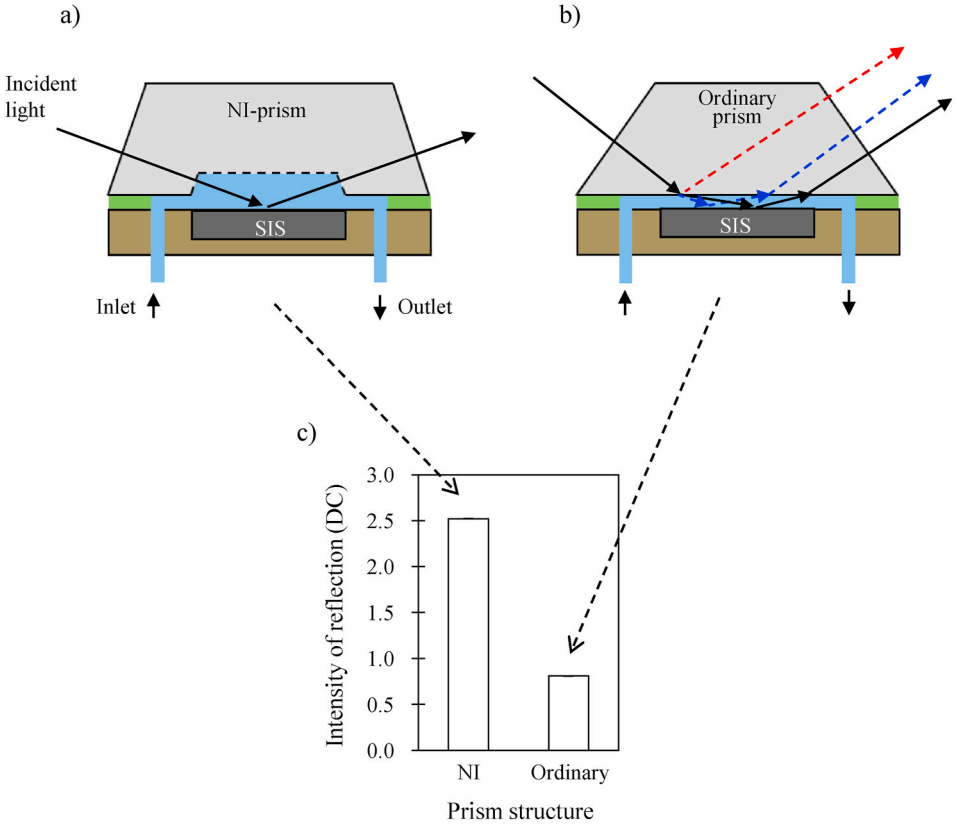

Fig. 2. Effect of NI-prism in improving a reflectance efficiency of probing beam. (a) Vertical cross-section of NI–SIS sensor assembly. NI-prism maintains the constant angle of incidence during sensor operation close to the Brewster angle at 72.4° in our case and removes the light beam reflected from the inner prism surface. (b) Vertical cross-section of the SIS sensor with ordinary-prism. Interference noise by the reflected light from the prism surface is the severe problem in this design (red dashed line.) The analytical errors are simply induced from incidence angle variations produced by refractive index changes of surrounding mediums (blue dashed line). (c) The reflected light intensities from the sensor surface were compared with the NI- and ordinary-prism SIS sensors, nearly three times increase in intensity. (For interpretation of the references to color in this figure legend, the reader is referred to the Web version of this article.)

transmission of the probing beam and significantly enhances the signal-to-noise ratio, acts as a signal amplifier, as shown in Fig. 2c (~3 times), which will help to improve sensitivity and achieve ultra-low detection limits.

3.3. Sensor chip and binding events detection process optimization

The effect of SiO_2 layer thickness over the sensor chip on the analytical performance of NI–SIS sensors was tested from experiments and simulations. Two sensor chips, one with native SiO_2 (~2 nm) and another with thermally grown SiO_2 (~52.4 nm) were used, we call it N–SiO_2 and T-SiO_2 sensor chips. The dextran SAM coated N–SiO_2 and T-SiO_2 sensor chips were loaded in the NI–SIS sensor assembly, and sensor performance was measured under a continuous flow of buffer solution at room temperature, plotted in Fig. 3a. The sensor with the T-SiO_2 chip shows a very noisy signal as compared to the N–SiO_2 sensor. The NI–SIS with N–SiO_2 chip has provided a superior precision of ±0.0001 for the sensing signals. To understand the above effect; uncoated and SAM-modified N–SiO_2 and T-SiO_2 sensor chips were measured using spectroscopic ellipsometry on several points. Thickness and surface roughness values of SiO_2, silane, and dextran thin films were obtained by inverting experimental data by multilayer modeling, listed in Table S1. Thermally grown SiO_2 films show nearly ten to fifteen-times higher surface roughness than native SiO_2, which transmit to sequentially grown silane and dextran over-layers on SiO_2. The thermal oxidation process grows island type silica cluster (Lepeshkin et al., 2016; Nikitin and Khriachtchev, 2015), gives a higher surface roughness. The rough sensor surface with a non-uniform growth of silane and dextran induces local pressure and temperature fluctuates within a sensing spot, which then fluctuates the local refractive index of an interface, which in-results could generate a noisy sensor signal.

The effect of surface roughness over the sensor surface was simulated via locally changing RI of the sensor chip surrounding medium. The simulation analysis was applied using WVASE32 software from J.A. Woollam co. A multilayer modeling was performed for a buffer solution/dextran/silane/SiO_2/Si structure. The Ψ signal was generated by calculating the Fresnel coefficient for various SiO_2 thickness in the above-said model (Diware et al., 2017b; Nestler and Helm, 2017). The simulation was performed under the assumption that the sensor is in ideal condition means only buffer solution is flowing over the N–SiO_2 and T-SiO_2 sensor chips. Thermal noise was induced by changing RI of the surrounding medium by ± 0.001, which is equivalent to ±10 °C temperature change (Nizamov and Mirsky, 2011). Fig. 3b and c shows the simulation results; there are no noticeable changes in signal for the N–SiO_2 sensor chip, while the T-SiO_2 sensor shows a shift in the base signal by ~0.081 at Brewster angle, which is way above the actual binding signal for analytes. This suggests that sensor chips having thicker SiO_2 layer induces higher thermal noise and masks the analyte signal. The chip with a native oxide layer has several advantages: cost-effective and easy use without surface treatment processes for elimination or deposition of an additional oxide layer.

The monoclonal antibody of cTnI was immobilized covalently on dextran activated sensor chip containing carboxyl groups to measure the affinity binding for different concentrations of cTnI analyte. The capture antibody was investigated to analytical specificity for negative controls with structurally homogeneous molecules (Kim et al., 2012), and the growth dynamics showing strong binding of the antibody with sensor surface were in-situ monitored, plotted in Fig. S3a and b. The remaining reactive sites after antibody immobilization was blocked by flowing ethanolamine to avoid any non-specific binding (NBS). The analytical capability of ordinary prism SIS (Diware et al., 2015) and NI–SIS sensors was compared, shown in Fig. 4a. The cTnI antigen of 10 pg/mL in PBS was flown over both the sensor in the same environmental conditions. The NI–SIS sensors yield an approximately two times higher signal, enable highly sensitive measurements of low concentrations of cTnI. These biosensing capabilities are enhanced by eliminating the noise-induced from a beam reflected from the prism surface and reducing variations of the incidence angle of the laser from refractive index changes of surrounding environments. The higher intensity of the laser beam reflected from the chip surface of NI-SIS also supports increasing the signal-to-noise ratio for the cTnI sample. Sensorgrams for increasing concentrations of cTnI antigen are shown in Fig. 4b, signal increase with every injection of cTnI antigen and saturates, suggest the availability of enough binding sites.

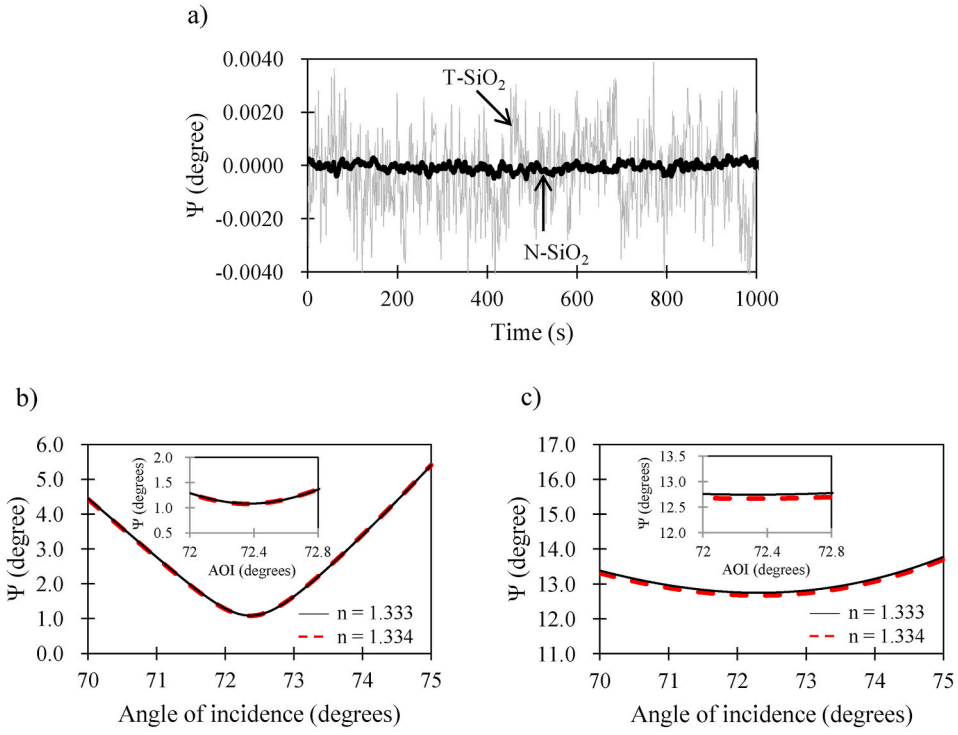

Fig. 3. Effect of SiO_2 thickness. (a) Experimentally measured Ψ signal for the dextran-coated N–SiO_2 and T-SiO_2 chip under a continuous flow of buffer solution at constant room temperature. The N–SiO_2 sensor chip shows a stable signal. (b) and (c) simulation results for the N–SiO_2 and T-SiO_2 sensor chips. Multilayer calculation was performed by considering ideal sensor operation conditions. Temperature fluctuation was introduced varying RI by ± 0.001, which is equivalent to ±10 K. The Ψ signal for (b) N–SiO_2 shows no variation while (c) T-SiO_2 (52.4 nm) sensor signal shift up to 0.081 from basal signals at Brewster angle.

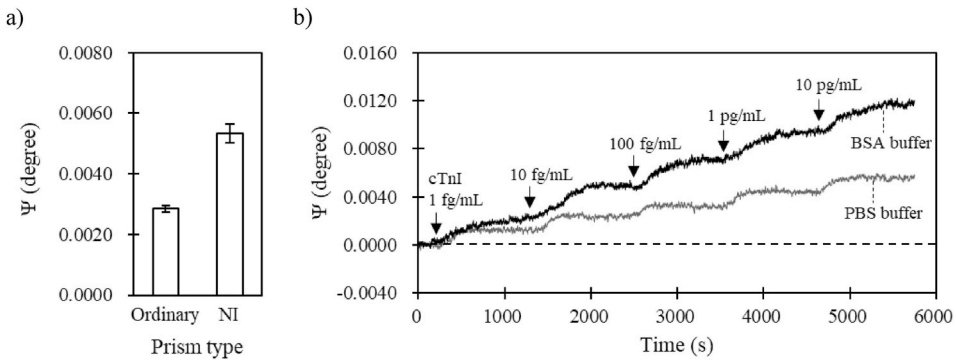

Fig. 4. Biosensing capability of NI–SIS system to cTnI. (a) NI–SIS sensor generates approximately two-folds higher Ψ signals for cTnI dose of 10 pg/mL diluted in PBS than that in the SIS sensor with ordinary-prism. (b) The analytical performance of NI–SIS was investigated by continuous measurements for various cTnI concentrations from 1 fg/mL to 10 ng/mL in buffer solutions of PBS and BSA-PBS, respectively.

The effect of buffer solution was tested; the PBS and mixture of PBS and BSA were used. The NI–SIS sensor performance is enhanced up to 47% in the PBS-BSA medium as compared to the PBS medium, shown in Fig. 4b. The BSA molecule might affect an increase of binding efficiency of cTnI antigen to the antibody as well as a minimization of NSB, reducing the background noise (Ahirwar et al., 2015; Jeyachandran et al., 2010; Schonheyder and Andersen, 1984). It can also enhance a specific activity of the antibody by eliminating the immunoglobulin to albumin components contained in human serum through the addition of BSA to a serum diluent (Schonheyder and Andersen, 1984).

3.4. Analytical performance in human serum

Non-specific binding is a severe issue in biosensing, especially for analytes in human serum. Background noise from the serum components masks the actual analyte signal. We tested three NSB sites blocking agents; ethanolamine, BSA, and casein, shown in Fig. S4. Ethanolamine is commonly used to chemically quench the remaining active carboxyl groups after immobilization of the antibody (Chu et al., 2014), gives a very noisy Ψ signal, suggests physical adsorption of the serum constituents. While BSA shows ~70 times reduction in the noise than ethanolamine and casein gives 8.1% less noisy signal than BSA by effectively reducing hydrophobic, ionic, and electrostatic interactions between sensor chip and serum constituents (Buchwalow et al., 2011; Reimhult et al., 2008). These results suggest that BSA and casein effectively block the residual binding sites and remove NSB of heavy serum constitutes, and improves the signal-to-noise ratio.

To construct the dose-response curve, we first prepared the serum samples with cTnI in a range of 10 fg/mL–100 ng/mL, and the samples were then diluted 10-folds with the pretreatment solution to measure cTnI concentrations accurately regardless of matrix effect by serum components. The binding events over the sensor surface of each sample were continuously measured, shown in Fig. 5a. The signals were produced by subtracting non-specific values of normal serum, and then the

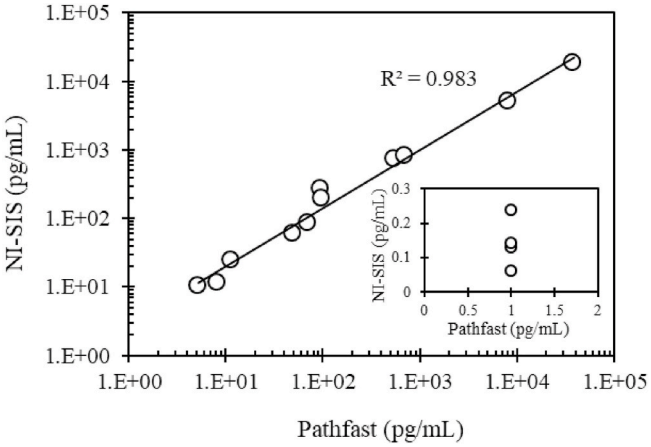

Fig. 6. Analytical correlation of NI–SIS sensor with the Pathfast reference system. The serum samples with the cTnI antigen were analyzed simultaneously using NI–SIS and the Pathfast analyzer, showing $R^2 > 0.98$ in a range between 5 pg/mL and 20 ng/mL. The detection range of the Pathfast was limited to 1 pg/mL, while the NI–SIS sensor shows a much lower detection limit, shown in the inset.

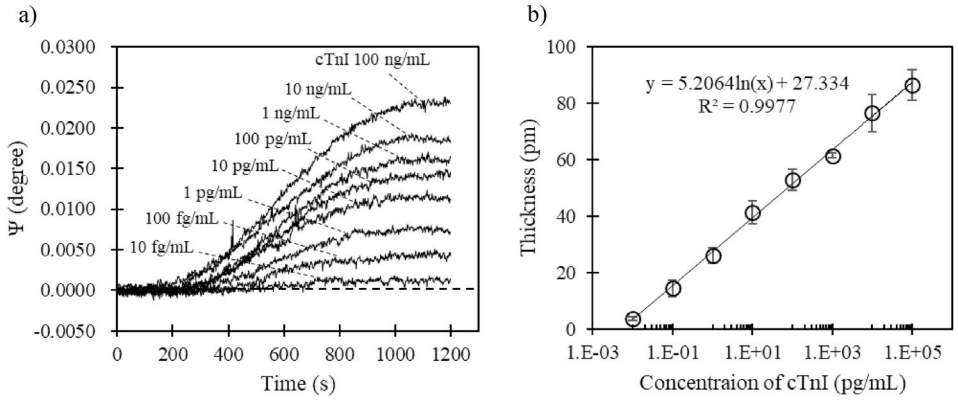

Fig. 5. The dose-response curve in human serum. (a) Measured Ψ signals for cTnI antigen of a concentration range from 10 fg/mL to 100 ng/mL in human serum. Plotted Ψ values were obtained by subtracting a non-specific value of normal serum. (b) The thickness values of NI–SIS were translated from the Ψ values of saturated signals for each concentration.

dose-response was obtained with the averaged value for the bound complex of cTnI. The Ψ can be linearly translated to the thickness of the thin bio-film, where Ψ value changes by 0.2583 at the Brewster angle for 1 nm variations of over-layer thickness for the 520 nm wavelength of incident light (Diware et al., 2015).

The growing thickness of the biomolecular layer over the NI–SIS sensor chip shows linear dependence for the given concentration range, plotted in Fig. 5b against the dose of each sample and the dose-response curve was analyzed by a logarithmic scale. We applied a linear regression analysis to obtain linearity ($R^2 > 0.99$) for wide dynamic ranges from 10 fg/mL to 100 ng/mL. The coefficient of variation for triplicate measurements was <22.3%. The reliability of the NI–SIS sensor was further estimated by a spike-and-recovery assessment. The responses of spiked concentrations of 100 fg/mL-10 ng/mL cTnI were fitted to the dose-response curve, obtained with recovery values between 70% and 144%. The detection limit of 22.0 fg/mL was obtained for the cTnI analytes in human serum as the concentrations corresponding to the blank value obtained by simply three times the standard deviation of Ψ signals in normal serum (Martens and Bienstman, 2019; Shrivastava and Gupta, 2011). These analytical performances can cover sufficiently clinical cut-off (<0.1 ng/mL) of cTnI (Madsen et al., 2006) without any labeling process for the signal enhancements.

To evaluate the correlation: the serum samples with the cTnI between 5 pg/mL and 20 ng/mL were first measured simultaneously on the NI–SIS sensor and Pathfast, respectively. The dose measured by two systems was linearly regressed by a log-log plot, providing a high correlation ($R^2 > 0.98$), as shown in Fig. 6. The dynamic range of the Pathfast system (Di Serio et al., 2009) was limited 1 pg/mL, lower than our current work (see inset in Fig. 6). This result strongly indicated that the SIS sensor could provide ultra-sensitive measurement enabling early diagnostics of AMI.

4. Conclusions

In conclusion, an ultra-high sensitive and label-free NI–SIS sensor was fabricated to detect cardiac-specific biomarkers at the early stage after AMI onset. NI–SIS sensor is equipped with a specially designed prism that provides the constant angle of incidence of probing beam close to NRC regardless of refractive index changes during operations. NI-prism improves the signal-to-noise ratio by eliminating a stray light reflected from the prism surface, resulting in ultra-high sensitive measurements for an extremely low concentration of cTnI analytes in the serum environment. Uniform and smooth SiO_2 layer on the sensor chip help to remove noise induced by local temperature and pressure variations in a sensing part. BSA and casein showed better blocking capability for residual binding sites. NI–SIS sensor shows superior analytical performances with a detection limit of 22.0 fg/mL. These systems require the evaluation of intra- and inter-assay variations and recovery rates in clinical samples. The label-free manner is useful to detect the fluctuations of analyte concentrations in real-time, which might be applied to continuous biosensing enabling companion diagnostics with rapid and effective treatments for certain diseases at the incipient stage (Jørgensen and Hersom, 2016; Kim et al., 2014; Papadopoulos et al., 2006). In future work, we will test the biosensing capabilities of the NI–SIS technique for simultaneous detections of different biomarkers that can improve the analytical accuracy and speed of disease diagnostics. The NI–SIS sensors have great potential in drug discovery, food contaminations, and the healthcare industry.

Credit (contributor roles taxonomy) author statement

Dong Hyung Kim: Conceptualization, Methodology, Formal analysis, Writing - Original Draft. Won Chegal: Software, Validation, Investigation, Visualization. Yong Jai Cho: Data Curation, Formal analysis. Sang Won O: Investigation, Resources. Long Van Le: Validation. Mangesh S. Diware: Writing - Original Draft. Se-Hwan Paek: Validation. Young Dong Kim: Investigation. Hyun Mo Cho: Conceptualization, Methodology, Writing - Review & Editing.

Declaration of competing interest

The authors declare that they have no known competing financial interests or personal relationships that could have appeared to influence the work reported in this paper.

Acknowledgments

This research was supported by the Research on National Measurement Standards Policy and Collaboration funded by Korea Research Institute of Standards and Science (KRISS – 2020 – GP2020-0013) and the Industrial Strategic Technology Development Program (Grant No. 10064060) funded by the Ministry of Trade, Industry & Energy (MI, Korea).

Appendix A. Supplementary data

Supplementary data to this article can be found online at https://doi.org/10.1016/j.bios.2020.112525.

References

Ahirwar, R., Bariar, S., Balakrishnan, A., Nahar, P., 2015. RSC Adv. 5 (121), 100077–100083.
Aissaoui, N., Bergaoui, L., Landoulsi, J., Lambert, J.-F., Boujday, S., 2012. Langmuir 28 (1), 656–665.
Bader, G., Ashrit, P.V., Truong, V.-V., 1998. Appl. Optic. 37 (7), 1146–1151.
Bidin, M.Z., Shah, A.M., Stanslas, J., Seong, C.L.T., 2019. Clinica chimica acta. Int. J. Clin. Chem. 495, 239–250.
Buchwalow, I., Samoilova, V., Boecker, W., Tiemann, M., 2011. Sci. Rep. 1, 28.
Cho, I.H., Lee, J., Kim, J., Kang, M.S., Paik, J.K., Ku, S., Cho, H.M., Irudayaraj, J., Kim, D. H., 2018. Sensors (Basel, Switzerland) 18 (1).
Cho, Y.J., Chegal, W., Lee, J.P., Cho, H.M., 2016. Opt. Express 24 (23), 26215–26227.
Chu, R., Reczek, D., Brondyk, W., 2014. Sci. Rep. 4, 7360.
Deng, Y., Nie, J., Zhang, X.H., Zhao, M.Z., Zhou, Y.L., Zhang, X.X., 2014. Analyst 139 (13), 3378–3383.
Di Serio, F., Caputo, M., Zaninotto, M., Ottomano, C., Plebani, M., 2009. Clin. Chem. Lab. Med. 47 (7), 829–833.
Diware, M., Cho, H., Chegal, W., Cho, Y., O, S., Paek, S.-H., Kim, D., Kim, K.-S., Min, Y., Jo, J., Shin, C., 2017a. Biointerphases 12, 01A402.
Diware, M.S., Cho, H.M., Chegal, W., Cho, Y.J., Jo, J.H., O, S.W., Paek, S.H., Yoon, Y.H., Kim, D., 2015. Analyst 140 (3), 706–709.
Diware, M.S., Cho, H.M., Chegal, W., Cho, Y.J., Kim, D.S., O, S.W., Kim, K.S., Paek, S.H., 2017b. Biosens. Bioelectron. 87, 242–248.
Dung, T.T., Lee, U.J., Kim, M.H., Kim, K.E., Cho, H.M., Fermin, C.D., Kim, D.H., Kim, M., 2019. Biosens. Bioelectron. 141, 111469.
Esfandyarpour, R., Esfandyarpour, H., Javanmard, M., Harris, J.S., Davis, R.W., 2013. Sensor. Actuator. B Chem. 177, 848–855.
Hasic, S., Jadric, R., Kiseljakovic, E., Radovanovic, J., Winterhalter-Jadric, M., 2006. Bosn. J. Basic Med. Sci. 6 (1), 19–23.
Hofmann, R., James, S.K., Jernberg, T., Lindahl, B., Erlinge, D., Witt, N., Arefalk, G., Frick, M., Alfredsson, J., Nilsson, L., Ravn-Fischer, A., Omerovic, E., Kellerth, T., Sparv, D., Ekelund, U., Linder, R., Ekström, M., Lauermann, J., Haaga, U., Pernow, J., Östlund, O., Herlitz, J., Svensson, L., 2017. N. Engl. J. Med. 377 (13), 1240–1249.
Jørgensen, J.T., Hersom, M., 2016. Ann. Transl. Med. 4 (24), 482.
Jeyachandran, Y.L., Mielczarski, J.A., Mielczarski, E., Rai, B., 2010. J. Colloid Interface Sci. 341 (1), 136–142.
Keller, T., Zeller, T., Peetz, D., Tzikas, S., Roth, A., Czyz, E., Bickel, C., Baldus, S., Warnholtz, A., Frohlich, M., Sinning, C.R., Eleftheriadis, M.S., Wild, P.S., Schnabel, R.B., Lubos, E., Jachmann, N., Genth-Zotz, S., Post, F., Nicaud, V., Tiret, L., Lackner, K.J., Munzel, T.F., Blankenberg, S., 2009. N. Engl. J. Med. 361 (9), 868–877.
Kim, D.H., Paek, S.H., Lim, G.S., Jeon, J.W., Paek, S.H., 2012. Anal. Biochem. 431 (1), 11–18.
Kim, D.H., Seo, S.M., Cho, H.M., Hong, S.J., Lim, D.S., Paek, S.H., 2014. Biosens. Bioelectron. 62, 234–241.
Kim, E., Baaske, M.D., Vollmer, F., 2017. Lab Chip 17 (7), 1190–1205.
Lai, G., Cheng, H., Xin, D., Zhang, H., Yu, A., 2016. Anal. Chim. Acta 902, 189–195.
Lee, B.H., Kim, S.H., Ko, Y., Park, J.C., Ji, S., Gu, M.B., 2019. Biosens. Bioelectron. 126, 122–128.
Lepeshkin, S., Baturin, V., Tikhonov, E., Matsko, N., Uspenskii, Y., Naumova, A., Feya, O., Schoonen, M.A., Oganov, A.R., 2016. Nanoscale 8 (44), 18616–18620.
Lewandrowski, K., Chen, A., Januzzi, J., 2002. Am. J. Clin. Pathol. 118 (Suppl. l), S93–S99.

Li, K., Wang, S., Wang, L., Yu, H., Jing, N., Xue, R., Wang, Z., 2018. Sensors 18 (1), 15.
Lim, G.-S., Seo, S.-M., Paek, S.-H., Kim, S.-W., Jeon, J.-W., Kim, D.-H., Cho, I.-H., Paek, S.-H., 2015. Sci. Rep. 5, 14848.
Liu, Y., Chen, S., Liu, Q., Masson, J.-F., Peng, W., 2015. Opt. Express 23, 20540–20548.
Madsen, L.H., Christensen, G., Lund, T., Serebruany, V.L., Granger, C.B., Hoen, I., Grieg, Z., Alexander, J.H., Jaffe, A.S., Van Eyk, J.E., Atar, D., 2006. Circ. Res. 99 (10), 1141–1147.
Martens, D., Bienstman, P., 2019. Sci. Rep. 9 (1), 5767.
Minamikawa, T., Hsieh, Y.-D., Shibuya, K., Hase, E., Kaneoka, Y., Okubo, S., Inaba, H., Mizutani, Y., Yamamoto, H., Iwata, T., Yasui, T., 2017. Nat. Commun. 8 (1), 610.
Morrow, D.A., Antman, E.M., Tanasijevic, M., Rifai, N., de Lemos, J.A., McCabe, C.H., Cannon, C.P., Braunwald, E., 2000. J. Am. Coll. Cardiol. 36 (6), 1812–1817.
Nestler, P., Helm, C.A., 2017. Opt. Express 25 (22), 27077–27085.
Nikitin, T., Khriachtchev, L., 2015. Nanomaterials (Basel, Switzerland) 5 (2), 614–655.
Nizamov, S., Mirsky, V.M., 2011. Biosens. Bioelectron. 28 (1), 263–269.
Ortiz-Riaño, E.J., Avila-Huerta, M.D., Mancera-Zapata, D.L., Morales-Narváez, E., 2020. Biosens. Bioelectron. 165, 112319.
Ostroff, R.M., Maul, D., Bogart, G.R., Yang, S., Christian, J., Hopkins, D., Clark, D., Trotter, B., Moddel, G., 1998. Clin. Chem. 44 (9), 2031–2035.
Papadopoulos, N., Kinzler, K.W., Vogelstein, B., 2006. Nat. Biotechnol. 24 (8), 985–995.
Reimhult, K., Petersson, K., Krozer, A., 2008. Langmuir 24 (16), 8695–8700.
Schonheyder, H., Andersen, P., 1984. J. Immunol. Methods 72 (1), 251–259.
Seo, S.M., Kim, S.W., Park, J.N., Cho, J.H., Kim, H.S., Paek, S.H., 2016. Biosens. Bioelectron. 83, 19–26.
Shi, J., Chan, C., Pang, Y., Ye, W., Tian, F., Lyu, J., Zhang, Y., Yang, M., 2015. Biosens. Bioelectron. 67, 595–600.
Shrivastava, A., Gupta, V., 2011. Chronicles Young Sci. 2 (1), 21–25.
Tan, Y., Wang, Y., Li, M., Ye, X., Wu, T., Li, C., 2017. Biosens. Bioelectron. 91, 741–746.
Xiao, X., Gao, Y., Xiang, J., Zhou, F., 2010. Anal. Chim. Acta 676 (1–2), 75–80.
Yanase, Y., Hiragun, T., Kaneko, S., Gould, H.J., Greaves, M.W., Hide, M., 2010. Biosens. Bioelectron. 26 (2), 674–681.
Yola, M.L., Atar, N., 2019. Biosens. Bioelectron. 126, 418–424.